Geophysical Journal International

Geophys. J. Int. (2012) **188,** 1382–1392 doi: 10.1111/j.1365-246X.2011.05344.x

Structure-preserving modelling of elastic waves: a symplectic discrete singular convolution differentiator method

Xiaofan Li, Wenshuai Wang, Mingwen Lu, Meigen Zhang and Yiqiong Li

Key Laboratory of the Earth's Deep Interior, CAS, Institute of Geology and Geophysics, Chinese Academy of Sciences, Beijing 100029, *China.*
E-mail: xflee@mail.iggcas.ac.cn

Accepted 2011 December 18. Received 2011 December 16; in original form 2011 March 10

SUMMARY

In this paper, we introduce the so-called symplectic discrete singular convolution differentiator (SDSCD) method for structure-preserving modelling of elastic waves. In the method presented, physical space is discretized by the DSCD, whereas an explicit third-order symplectic scheme is used for the time discretization. This approach uses optimization and truncation to form a localized operator. This preserves the fine structure of the wavefield in complex media and avoids non-causal interaction when parameter discontinuities are present in the medium. Theoretically, the approach presented is a structure-preserving algorithm. Also, some numerical experiments are shown in this paper. Elastic wavefield modelling experiments on a laterally heterogeneous medium with high parameter contrasts demonstrate the superior performance of the SDSCD for suppression of numerical dispersion. Long-term computational experiments exhibit the remarkable capability of the approach presented for long-time simulations. Promising numerical results suggest the SDSCD is suitable for high-precision and long-time numerical simulations, as it has structure-preserving property and it can suppress effectively numerical dispersion when coarse grids are used.

Key words: Numerical solutions; Numerical approximations and analysis; Body waves; Computational seismology; Wave propagation.

INTRODUCTION

High-precision elastic wave modelling becomes increasingly important due to demands for seismological research and seismic exploration. Especially, high-precision or long-time modelling of seismic wave propagation is required when dealing with seismic wave propagation in highly heterogeneous media, seismic wave inversion, high-resolution seismic wave imaging, and long-time modelling of seismic wave is required for Earth's free oscillations modelling and seismic noise propagation modelling. Generally, seismic modelling methods can be classified into three categories: direct methods, integral-equation methods and ray tracing methods. Carcione *et al*. (2002) gave a classical review of these methods. In this paper, emphasis is placed on direct methods.

Modelling seismic waves in the time domain using direct methods involves discretization of both space and time derivatives. In the past tens years, the traditional finite difference methods (non-symplectic schemes) for temporal discretizations has been widely used. Because the classical finite difference methods for temporal discretizations are not structure-preserving schemes, it is extremely difficult to avoid accumulated errors in precise or long-time numerical simulations for partial differential equations using these methods. When solving differential equations numerically, some numerical algorithms can preserve the corresponding structures. This can be called the structure-preserving property of a numerical algorithm. The structure-preserving property of symplectic algorithms is well known. Theoretically, a numerical method for Hamiltonian dynamical systems can be called a symplectic algorithm if the resulting numerical solution is also a symplectic mapping. Some symplectic algorithms for partial differential equations have been developed and used, such as Lax–Wendroff methods (Lax & Wendroff 1960; Carcione *et al.* 2002) and Nyström methods (Qin & Zhu 1991; Okunbor & Skeel 1992; Calvo & Sanz-Serna 1993; Hairer *et al.* 1993; Tsitouras 1999; Blanes & Moan 2002; Lunk & Simen 2005). Chen (2009) discussed the structure-preserving property of Lax–Wendroff and Nyström methods in detail.

The most widely used direct methods for spatial discretizations are: classical finite difference (FD) methods (Claerbout 1985; Bayliss *et al.* 1986; Levander 1988), pseudospectral methods (Gazdag 1981) and finite element methods (Ciarlet & Lions 1991). Some optimized methods or combinations of these methods are also available, such as optimized finite difference methods (Holberg 1987; Geller & Takeuchi 1998; Takeuchi & Geller 2000; Moczo *et al.* 2002), convolution differentiator methods (Zhou & Greenhalgh 1992; Mora 1986; Etgen 1987; Yomogida & Etgen 1993),

spectral element methods (Komatitsch & Tromp 2002; Komatitsch & Vilotte 1998) and finite volume methods (Dormy & Tarantola 1995). Each of these methods has its merits and drawbacks. For spatial discretizations, a powerfully spatial derivative operator is one of keys to solve wave equations for strongly heterogeneous media. Most effort has been focused on developing either global methods (Fornberg 1990; Chen 1996; Zhao *et al*. 2003) or localized methods (Bayliss *et al*. 1986; Mora 1986; Etgen 1987; Holberg 1987; Zhou & Greenhalgh 1992; Yomogida & Etgen 1993; Levander 1988; Komatitsch & Vilotte 1998; Geller & Takeuchi 1998; Takeuchi & Geller 2000; Moczo *et al.* 2002; Komatitsch & Tromp 2002; Yang *et al*. 2004) for solving partial differential equations. Generally, the local methods (e.g. methods of finite difference, finite volumes and finite elements) are highly localized in the spatial domain, yet delocalized in their spectral domain; global methods, such as the Fourier spectral method, are highly localized in their spectral representations and delocalized in the spatial domain. As a consequence, global methods appear to be more accurate than local methods when they are used to approximate spatial derivatives of a smooth function. The main advantage of local methods is their flexibility for satisfying special boundary conditions and for treating complex geometries. In this paper, we elect a discrete singular convolution differentiator (DSCD) with optimization and truncation for spatial discretizations of wave equations. This differentiator can be considered as a localized operator, though mathematical analysis (Qian 2003) indicates that the regularized Shannon delta kernel is a local spectral kernel. Numerical analysis (Feng & Wei 2002; Sun & Zhou 2006) indicates that the discrete singular convolution scheme can be more accurate than global methods (e.g. the Fourier pseudospectral methods) for treating non-bandlimited problems and for treating complex geometries (e.g. approximating spatial derivatives of discontinuous functions), even if it is not as accurate as global methods for approximating bandlimited periodic functions or for approximating spatial derivatives of smooth functions.

So far structure-preserving modelling methods for elastic wave equations are infrequent, but the sort of numerical method is required for high-precision seismic modelling, especially for long-time simulations of seismic wave propagation. Although the concept of the symplectic convolution differentiator seems not to be very new mathematically, it could be used to develop a new structure-preserving scheme for elastic wave equations modelling and any reference on similar research has not been found by far.

In this paper, we present a new method for accurately and efficiently modelling elastic wavefields and for long-time simulations of seismic wave propagation using a symplectic DSCD (SDSCD) algorithm. Here, a truncated and optimized DSCD is used for spatial discretizations. Theoretically, the DSCD is a localized operator that can both describe the fine structure of wavefields in complex media and avoid any non-causal interaction of the propagating wavefields when parameter discontinuities are present in the medium. The operator is truncated for practical implementation. Nine-point operators on regular grids are used as a compromise between computational efficiency and accuracy. To improve the capability of seismic modelling methods for long-time simulations, we substitute the third-order partitioned Runge–Kutta scheme (a symplectic algorithm) for traditional finite difference scheme in temporal discretizations. In numerical experiments described by this paper, we apply the SDSCD to elastic wavefield modelling in heterogeneous media and to long-time simulations of elastic wave propagating. Our numerical results indicate that the SDSCD is suitable for large-scale numerical modelling since it effectively suppresses numerical dispersion by discretizing the elastic wave equations when coarse grids are used. The numerical results also confirm that the SDSCD presented in this paper has the superior performance to solve long-time simulation problems.

THEORETICAL METHOD

Discrete singular convolution differentiator

In recent years, a DSCD for solving partial differential equations has been developed (Feng & Wei 2002; Sun & Zhou 2006). The differentiator can use optimization and truncation to form a localized operator. This is a high-precision and efficient operator to solve partial differential equations. In this paper, the DSCD will be elected for spatial differentiation. Here, we begin by summarizing the DSCD for the spatial derivative to solve wave equations. Let $\boldsymbol{T}(x-t)$ be a singular kernel and $\eta(x)$ be an element of the space of test function. A singular convolution is defined as

$$f(x) = (T * \eta)(x) = \int_{-\infty}^{\infty} T(x-t)\eta(t)\,\mathrm{d}t. \tag{1}$$

Here, singular kernels of the delta type are required

$$T(x) = \delta^{(q)}(x), \quad (q = 0, 1, 2, \ldots). \tag{2}$$

The singular kernel is $T(x) = \delta(x)$ of particular importance for interpolation of surfaces and curves. Higher-order kernels, $T(x) = \delta^{(q)}(x)$, $(q = 0, 1, 2, \ldots)$ are essential for numerically solving partial differential equations. However, one has to find appropriate approximations to the above singular kernel, which cannot be directly realized in computers. Finally, a sequence of approximations is considered as

$$\lim_{\alpha\to\alpha_0} \delta_\alpha^{(q)}(x) = \delta^{(q)}(x), \quad q = 0, 1, 2, \ldots, \tag{3}$$

where α is a parameter which characterizes the approximation with the α_0 being a generalized limit. Among various approximation kernels, regularized Shannon delta kernel (Gottlieb *et al*. 1981) is an excellent candidate. It can be written as

$$\delta_{\sigma,\Delta}(x) = \frac{\sin\frac{\pi}{\Delta}x}{\frac{\pi}{\Delta}x}\exp\left(-\frac{x^2}{2\sigma^2}\right). \tag{4}$$

In this formula, Δ is the grid spacing and σ determines the width of the Gaussian envelop. For a given $\sigma \neq 0$, the limit of $\Delta \to 0$ reproduces the delta kernel (distribution). With the regularized Shannon kernel, a function u and its nth order derivative can be approximated by a discrete convolution

$$u^{(q)}(x) \approx \sum_{k=\lceil x\rceil - W}^{\lceil x\rceil + W} \delta_{\sigma,\Delta}^{(q)}(x - x_k)u(x_k), \quad q = 0, 1, 2, \ldots, \tag{5}$$

where $\lceil x\rceil$ denotes the gridpoint that is closest to x, and $2W + 1$ is the computational bandwidth, or effective kernel support, which is usually smaller than the computational bandwidth of the spectral method, that is, the entire domain span. Generally, a larger W will lead to a higher accuracy. When $q = 1$, the fist order derivative $d_1(x)$ can be discretized as

$$d_1(k\Delta x) = \begin{cases} \delta'_{\sigma,\Delta}(k\Delta x) & k = \pm1, \pm2, \ldots, \pm W \\ 0 & k = 0 \end{cases}, \tag{6}$$

where Δx is the grid spacing. For practical implementation, the differentiator has to be truncated as a short operator, but doing so could lead to the Gibbs phenomenon. To avoid the Gibbs phenomenon, we use a Hanning window function for truncating the differentiator:

$$w(k) = \left[2\alpha - 1 + 2(1-\alpha)\cos^2\frac{k\pi}{2(W+2)}\right]^{\frac{\beta}{2}}, \quad k = 0, \pm1, \pm2, \ldots, W. \tag{7}$$

The constants $\alpha(0.5 \leq \alpha \leq 1)$ and β allow a family of different windows to be considered. A modified and practical convolutional differentiator can be denoted by

$$\hat{d}_1(k\Delta x) = \begin{cases} d_1(i\Delta x)w(i) & i = \pm1, \pm2, \ldots, \pm W \\ 0 & i = 0 \end{cases}. \tag{8}$$

From the discrete Fourier analysis of the discrete singular convolution (Feng & Wei 2002; Yang *et al*. 2002), it can be found the accuracy of the operator clearly depends on its length. The error analysis also indicates that the accuracy of the discrete singular convolution approximation to the derivative is controllable and can be better than the traditional higher-order finite difference approximation. To obtain an optimal balance between computational efficiency and accuracy of the discrete singular convolution approach, we chose nine-point explicit operators on regular grids via the discrete Fourier analysis. The nine-point explicit operator (DSCD) used in this paper is accurate eighth-order in space.

A symplectic scheme of temporal discretization for the elastic wave equations

For a 2-D isotropic elastic medium, the first-order velocity–stress hyperbolic system of elastic wave equations (Virieux 1986) can be written as

$$\begin{cases} \rho\frac{\partial v_x}{\partial t} = \frac{\partial \sigma_{xx}}{\partial x} + \frac{\partial \sigma_{xz}}{\partial z} + f_x, \\ \rho\frac{\partial v_z}{\partial t} = \frac{\partial \sigma_{zx}}{\partial x} + \frac{\partial \sigma_{zz}}{\partial z} + f_z, \\ \frac{\partial \sigma_{xx}}{\partial t} = (\lambda+2\mu)\frac{\partial v_x}{\partial x} + \lambda\frac{\partial v_z}{\partial z}, \\ \frac{\partial \sigma_{zz}}{\partial t} = \lambda\frac{\partial v_x}{\partial x} + (\lambda+2\mu)\frac{\partial v_z}{\partial z}, \\ \frac{\partial \sigma_{xz}}{\partial t} = \mu\frac{\partial v_x}{\partial z} + \mu\frac{\partial v_z}{\partial x}, \\ \frac{\partial \sigma_{zx}}{\partial t} = \mu\frac{\partial v_x}{\partial z} + \mu\frac{\partial v_z}{\partial x}, \end{cases} \tag{9}$$

where v_x and v_z are the velocity components of the x and z directions, σ_{xx}, σ_{zz} and σ_{xz} are the stress components, f_x and f_z are the body forces, λ and μ are the elastic parameters and ρ is the density. We write eq. (9) as the following matrix for easy expressing:

$$\frac{\mathrm{d}}{\mathrm{d}t}\begin{pmatrix} v \\ \sigma \end{pmatrix} = (P+Q)\begin{pmatrix} v \\ \sigma \end{pmatrix}, \tag{10}$$

where $v = (v_x, v_z)^T$, $\sigma = (\sigma_{xx}, \sigma_{zz}, \sigma_{xz}, \sigma_{zx})^T$

$$P = \begin{pmatrix} 0 & 0 & \frac{1}{\rho}\frac{\partial}{} & \partial x & 0 & \frac{1}{\rho}\frac{\partial}{\partial z}0 \\ 0 & 0 & 0 & \frac{1}{\rho}\frac{\partial}{\partial z} & 0 & \frac{1}{\rho}\frac{\partial}{\partial x} \\ 0 & 0 & 0 & 0 & 0 & 0 \\ 0 & 0 & 0 & 0 & 0 & 0 \\ 0 & 0 & 0 & 0 & 0 & 0 \\ 0 & 0 & 0 & 0 & 0 & 0 \end{pmatrix} \text{ and}$$

$$Q = \begin{pmatrix} 0 & 0 & 0 & 0 & 0 & 0 \\ 0 & 0 & 0 & 0 & 0 & 0 \\ (\lambda+2\mu)\frac{\partial}{\partial x} & \lambda\frac{\partial}{\partial z} & 0 & 0 & 0 & 0 \\ \lambda\frac{\partial}{\partial x} & (\lambda+2\mu)\frac{\partial}{\partial z} & 0 & 0 & 0 & 0 \\ \mu\frac{\partial}{\partial z} & \mu\frac{\partial}{\partial x} & 0 & 0 & 0 & 0 \\ \mu\frac{\partial}{\partial z} & \mu\frac{\partial}{\partial x} & 0 & 0 & 0 & 0 \end{pmatrix}.$$

For the time variable t, the solution of eq. (10) is

$$\begin{pmatrix} v(t) \\ \sigma(t) \end{pmatrix} = \exp[t(P+Q)]\begin{pmatrix} v(0) \\ \sigma(0) \end{pmatrix}, \tag{11}$$

where $v(0) = v(t)|_{t=0}$, $\sigma(0) = \sigma(t)|_{t=0}$.

When real numbers $c_i, d_i, i = 1, \cdots, k$ exist,

$$\exp(tP)\exp(tQ) = \prod_{i=1}^{k}\exp(c_i tP)\exp(d_i tQ) + O(t^{m+1}) \tag{12}$$

is true. Because $\exp(c_i tP)$ and $\exp(d_i tQ)$ are symplectic transformations (Chen & Qin 2000), kth-stage symplectic scheme with mth-order accuracy of eq. (11) can be obtained

$$\begin{pmatrix} v \\ \sigma \end{pmatrix}(t) = \prod_{i=1}^{k}\exp(c_i tP)\exp(d_i tQ)\begin{pmatrix} v \\ \sigma \end{pmatrix}(t) + O(t^{m+1}). \tag{13}$$

Here we call the real numbers in eq. (13) as symplecticity coefficients.

By the temporal discretization and Taylor expansion, the discrete scheme of eq. (13) can be denoted by

$$\begin{pmatrix} v^{(n+1)} \\ \sigma^{(n+1)} \end{pmatrix} = \prod_{i=1}^{k}(I + c_i\Delta t P)(I + d_i\Delta t Q)\begin{pmatrix} v^{(n)} \\ \sigma^{(n)} \end{pmatrix}, \tag{14}$$

where n is the index along the time axis, Δt is sampling rate along the time axis, i is the stage index of scheme (14). Because the temporal errors of eq. (13) is $O(t^{m+1})$, the temporal accuracy of eq. (14) is mth-order. Adopting methods which were given by Suzuki (1992) and Yoshida (1990) to eq. (14), the symplecticity coefficients for $k = m = 3$ are

$$c_1 = \frac{1}{12}\left(\sqrt{\frac{209}{2}} - 7\right), \quad c_2 = \frac{11}{12}, \quad c_3 = \frac{1}{12}\left(8 - \sqrt{\frac{209}{2}}\right),$$

$$d_1 = \frac{2}{9}\left(1 + \sqrt{\frac{38}{11}}\right), \quad d_2 = \frac{2}{9}\left(1 - \sqrt{\frac{38}{11}}\right), \quad d_3 = \frac{5}{9},$$

and eq. (14) can be written as

$$\begin{pmatrix} v^{(n+1)} \\ \sigma^{(n+1)} \end{pmatrix} = \prod_{i=1}^{3}(I + c_i\Delta t P)(I + d_i\Delta t Q)\begin{pmatrix} v^{(n)} \\ \sigma^{(n)} \end{pmatrix}. \tag{15}$$

The displacement can be written as

$$\mathbf{u}^{(n+1)} = \Delta t v^{(n+1)} + \mathbf{u}^{(n)}, \quad \mathbf{u}^{(n)} = \left(u_x^{(n)}, u_z^{(n)}\right), \tag{16}$$

where u_x and u_z are the displacement components of the x and z directions.

The above-mentioned coefficients (c_i and d_i) are identical with the solution of the symplecticity condition equations given by Iwatsu (2009) for a third-order symplectic integration method. Eq. (15) is a three-stage third-order explicit symplectic scheme for elastic wave equation modelling. The spatial derivatives in eq. (15) are calculated by the use of the DSCD (eq. 8). Iwatsu (2009) analysed computational precision and stability of the third-order symplectic temporal discretization scheme in detail. From his analysis, it can be seen that the above-mentioned temporal discretization scheme is far superior to non-symplectic temporal discretization schemes in computational precision and stability.

ACCURACY AND STABILITY CONDITION

Previous works generally evaluated the proposed computational schemes by presenting theoretical derivations or by conducting numerical tests for a homogeneous medium, using the numerical dispersion of the phase velocity as the criterion for evaluating accuracy. For SDSCD velocity-stress scheme, however, it is hard to obtain an explicit scheme for the grid-dispersion relations and its derivation is lengthy. Therefore, we use the following analyses of errors and waveform comparison to test the accuracy of numerical results, and the explicit scheme for the grid-dispersion relations will be given in a separate study.

To test the accuracy of numerical results from SDSCD (eqs 14, 15 and 16), the root-mean-square (rms) deviation E from the analytical solution given by De Hoop (1960) in a homogeneous space (Fig. 1) used for quantitative measurement of the numerical accuracy is defined as

$$E_k = \left\{ \frac{1}{MN} \sum_{i=1}^{M} \sum_{j=1}^{N} \left[{}_k u_{i,j}^n - u_k(t_n, x_i, z_j) \right]^2 \right\}^{1/2}, \quad k = x, z, \tag{17}$$

where ${}_k u_{i,j}^n, k = x, z$ denotes x or z component of the numerical displacement at gridpoint (x_i, z_j) and at time t_n, and $u_k(t_n, x_i, z_j)$ denotes x or z component of the analytical displacement at the same gridpoint and at the same time. For the rms error measurement, we set $M = N = 50$ which are the total grid numbers in the x and z directions. In the numerical calculation, the model parameter are a P-wave velocity of $V_P = 3000$ m s^{-1}, a S-wave velocity of $V_S = 2000$ m s^{-1} and a density of $\rho = 2000$ kg m^{-3}. The number of gridpoints is 256 × 256, the model size is 2550 m × 2550 m, and the receiver is located at $(x_r, z_r) = (1600$ m, -800 m). The spatial increments were 10 m and the time increment is 1 ms. An explosive source is located at $(x_s, z_s) = (2550$ m, 2550 m), which is a Ricker wavelet and can be written as

$$f_x = f_z = f(t)\delta(x - x_s, z - z_s), \tag{18}$$

where $f(t) = \{1 - 2[\pi f_0(t - t_0)]^2\} \exp\{-[\pi f_0(t - t_0)]^2\}$, f_0 is the dominant frequency and t_0 is starting time. This is a medium model without any type of absorbing or transmitted boundary conditions.

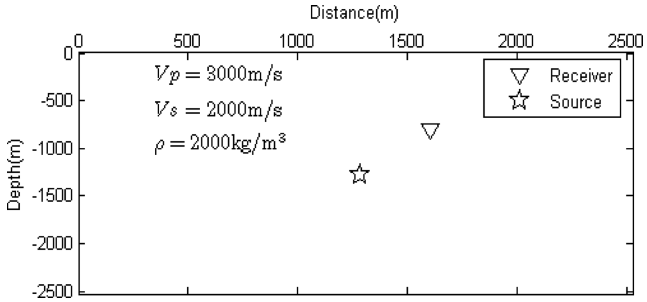

Figure 1. 2-D homogeneous medium model: configuration and parameters.

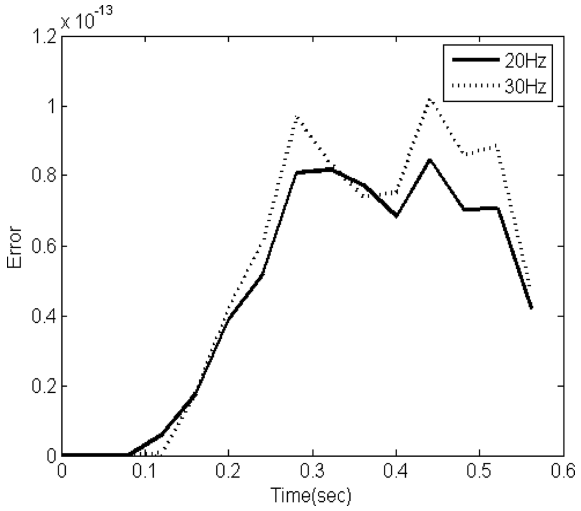

Figure 2. The errors of the SDSCD measured by the rms deviation E for the horizontal displacements.

Fig. 2 displays the computational results of the rms deviation E for the horizontal displacement generated by the SDSCD at different times and different dominant frequencies (20 and 30 Hz). The curves of the rms error indicates that the error introduced by the SDSCD measured by E decreases slightly with increasing of the dominant frequency f_0. Because the nine-point SDSCD selected in this paper is accurate eighth-order in space, we here compare it with the eighth-order FD operator. Fig. 3 shows the curves of the rms error at the dominant frequency of $f_0 = 30$ Hz for the nine-point SDSCD and for the eighth-order FD operator. From Fig. 3, it is found that the

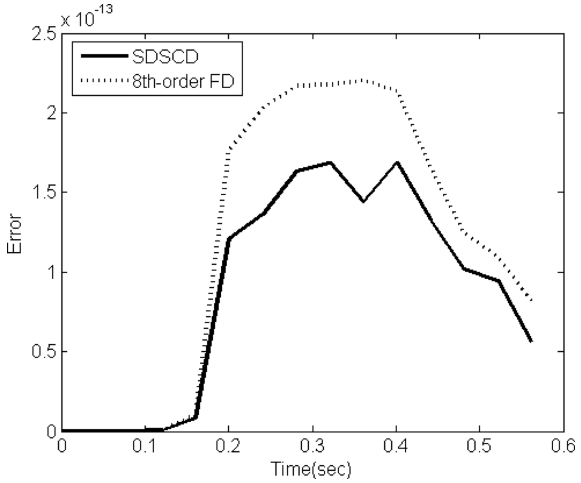

Figure 3. The errors of the SDSCD and the eighth-order FD operator measured by the rms deviation E for the vertical component. The explosive source $f_x = f_z = f(t)\delta(x - x_s, z - z_s)$ of Ricker wavelet with a frequency $f_0 = 30$ Hz is located at point (1600 m, -800 m).

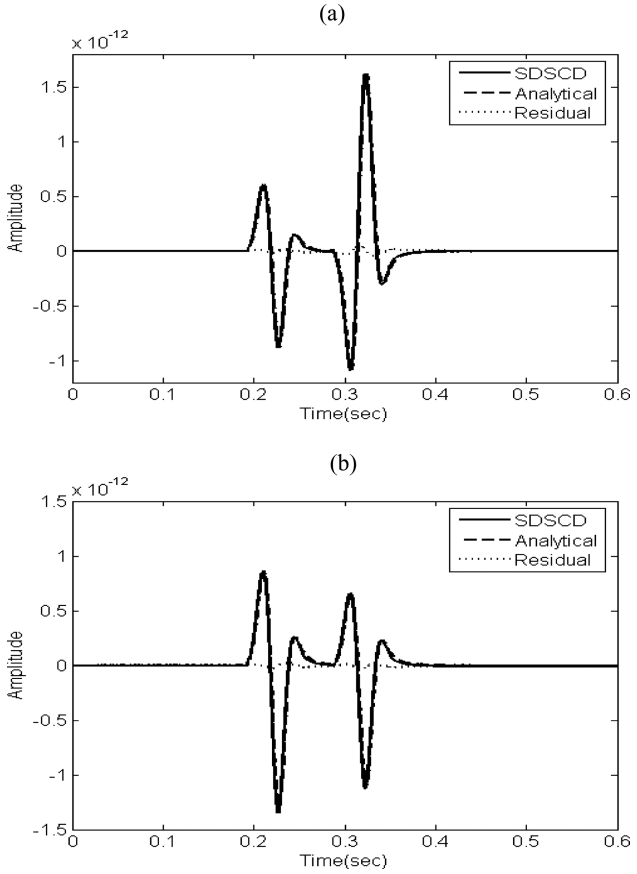

Figure 4. Comparison between the analytical displacements and numerical displacements generated by SDSCD. The explosive source $f_x = f_z = f\ (t)\ \delta(x - x_s, z - z_s)$ of Ricker wavelet with a frequency $f_0 = 25$ Hz is located at point (1600 m, −800 m). Panel (a) is a display for the horizontal components of the particle displacements, and panel (b) shows the vertical components of the particle displacements.

error of the nine-point SDSCD is less than that of the eighth-order FD operator. In average, the average error of the nine-point SDSCD is about 38.8 per cent of that of the eighth-order FD operator for short-time computations. More intuitively, a comparison between the analytical and numerical horizontal displacements at point (1600 m, −800 m) for the dominant frequency of $f_0 = 25$ Hz is shown in Fig. 4. It is found that the curves for the numerical solutions obtained by the nine-point SDSCD almost superimpos upon the curves for the analytical solutions.

Because it is very difficult to give an explicit treating for stability of the SDSCD velocity-stress scheme, the further theoretical stability condition will be analysed in a separate study. We here evaluate the stability using the Courant number $r = V_{\max}\Delta t/\Delta h$. Here $V_{\max}$ is the maximum value of *P*-wave velocity,$\Delta h = \Delta x = \Delta z$. For the above homogeneous medium (Fig. 1), the stability condition or the stability limit of eq. (16) is

$$\Delta t \leq 0.684\Delta h/V_p \quad \text{or maximum Courant number}$$
$$r_{\max} = \Delta t V_p/\Delta h \leq 0.684.$$

Maximum Courant number is a most common numerical stability condition. In the above-mentioned calculation of maximum Courant number, the model parameters are a *P*-wave velocity of $V_P = 3000$ m s^{-1}, a *S*-wave velocity of $V_S = 2000$ m s^{-1}. a density of $\rho = 2000$ kg m^{-3}, a spatial increment of $\Delta h = 10$ m and a maximum time increment of $\Delta t = 2.28$ ms.

Theoretically, the SDSCD approach is equivalent to an optimized FD method. Because of the use of eq. (15) and that of the nine-point SCD, the SDSCD approach is accurate third-order in time and eighth-order in space.

NUMERICAL EXPERIMENTS

Generally, the performance of numerical schemes is evaluated by considering the numerical dispersion as a function of number of gridpoints per wavelength. Even though the wave field in a highly heterogeneous medium is usually not known analytically, the overall performance can still be judged qualitatively. In this section, two numerical examples are given for evaluating the performance of the SDSCD approach.

The Fourier pseudospectral scheme is one of the most widely used methods, which is a high-precision scheme for treating uncomplicated geometries. We compared the numerical results found using SDSCD with those from Fourier pseudospectral scheme for a lateral heterogeneous medium with a high physical parameter contrast. The model consists of two different wave velocity regions separated by a rough curved interface (Fig. 5). The model parameters were a *P*-wave velocity of $V_{P1} = 2500$ m s^{-1}, a *S*-wave velocity of $V_{S1} = 1443$ m s^{-1} and a density of $\rho_1 = 2000$ kg m^{-3} for the upper layer with the pressure source, and a *P*-wave velocity of $V_{P2} = 4500$ m s^{-1}, a *S* wave velocity of $V_{S2} = 2589$ m s^{-1} and a density of $\rho_2 = 2600$ kg m^{-3} for the lower layer. The number of gridpoints was 256 × 256, the model size was 2550 m × 2550 m, and the wave source was located at point $(x_s, z_s) = (1280$ m, −1180 m). The receiver was located at point $(x_r, z_r) = (1280$ m, −1030 m). The spatial increments were 10 m and the time increment was 1 ms. The interface can be considered a velocity discontinuity since the velocity contrast is very high. The explosive source, a Ricker wavelet (it can be written as eq. 18), is located in the upper layer and has an amplitude spectrum peak at 30 Hz. To reduce the artificial reflections that are introduced by the edge of the computational grid, the non-reflecting boundary condition (Cerjan *et al*. 1985) was applied to the sides and bottom of the medium model.

Fig. 6(a) is elastic wavefield (vertical component) snapshots at time mark of 400 ms generated by the SDSCD. The snapshots in Figs 6(a) and (b) (generated by the Fourier pseudospectral scheme) clearly show the wave front of the direct *P* wave and other phases (e.g. the reflected *P*–*P* and *P*–*S* wave fronts, transmitted *P* and *P*–*S* wave fronts and scattered waves from the rough curved interface). The wave fronts are continuous and mend the physical parameter discontinuity in the model. From these snapshots, it can be seen that the wavefields simulated by SDSCD are very clear. There is hardly any grid dispersion despite the fact that there are only 4.81 grids or less per shortest wavelength at the dominant frequency (30 Hz). A similar phenomenon also appears when comparing the synthetic seismograms (Fig. 7a for the SDSCD and Fig. 7b for the Fourier pseudospectral scheme). The above-mentioned comparison indicates that the SDSCD scheme is as accurate as the Fourier pseudospectral scheme for short-time simulations and for treating uncomplicated geometries. Like the Fourier pseudospectral scheme, the SDSCD is suitable for large-scale numerical modelling with coarse spatial grids.

Based on these results, we conclude that the convolutional operator designed here is accurate to about 4.81 grids or less per shortest wavelength. Also, the SDSCD method effectively captures the inner interface without any special treatment at the discontinuity.

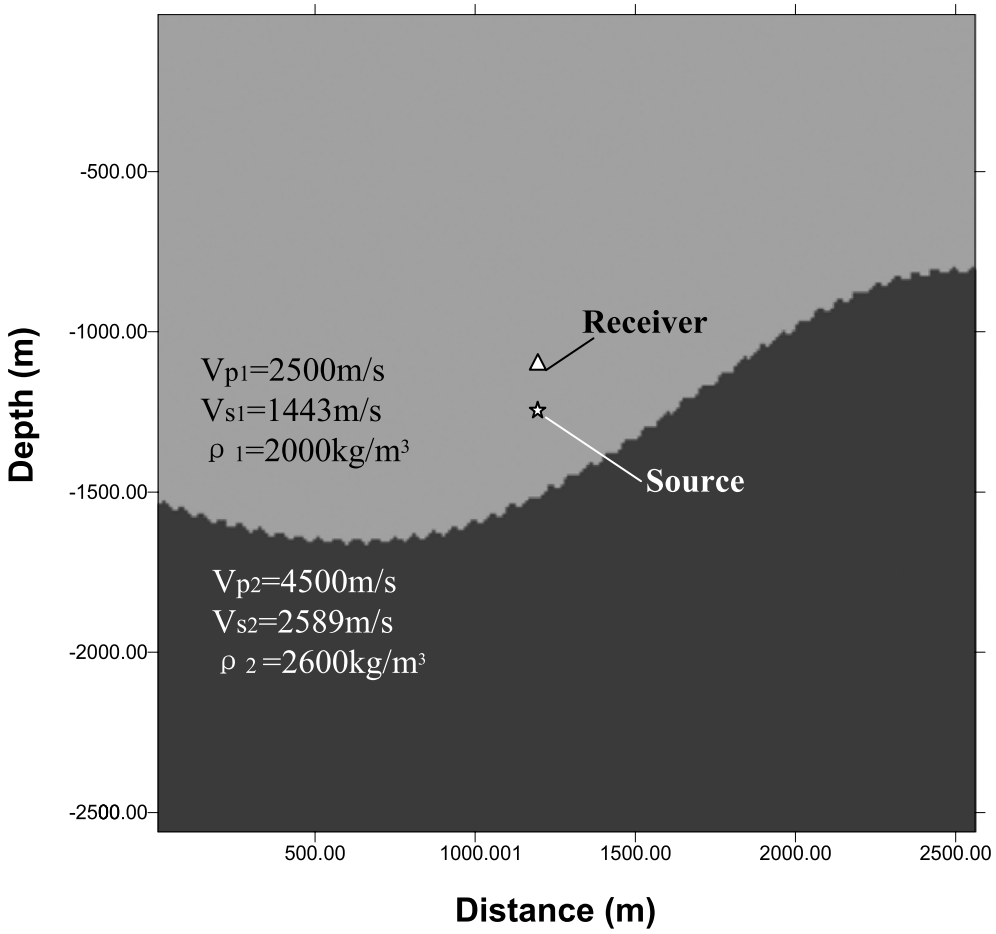

Figure 5. Lateral heterogeneous medium model: configuration and parameters.

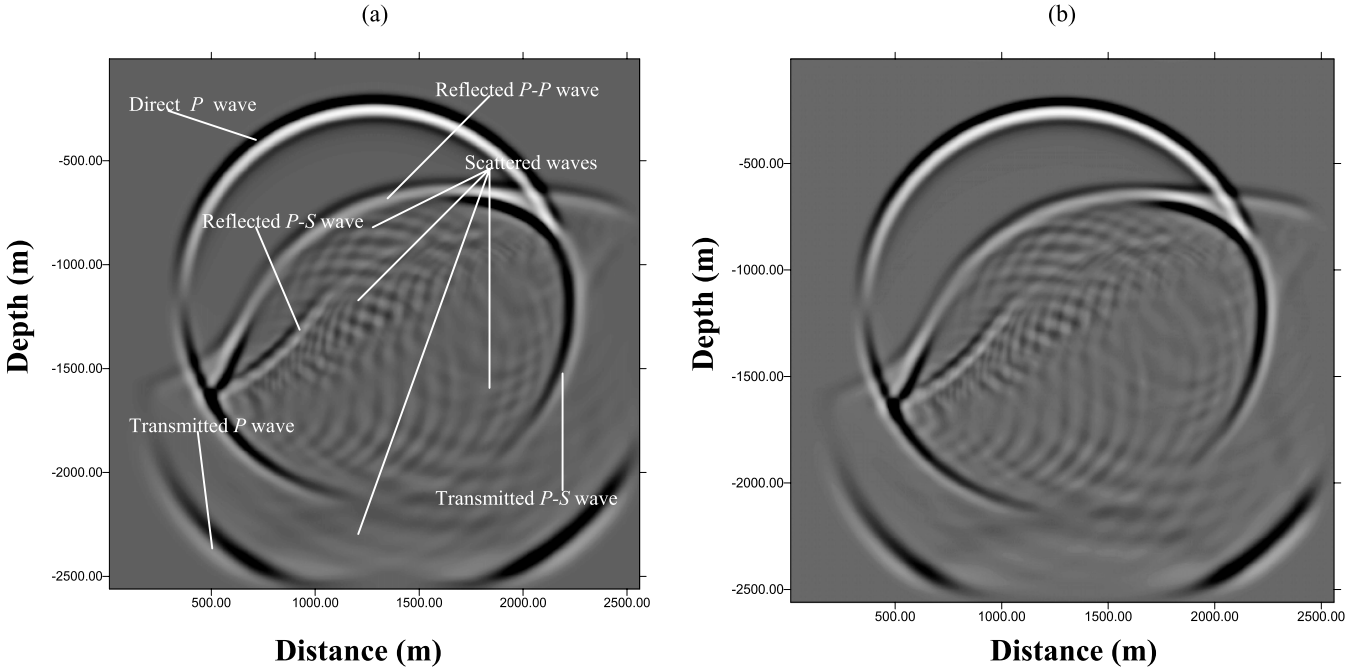

Figure 6. Snapshots of elastic wavefields (vertical component) in a lateral heterogeneous medium model at time 400 ms generated by SDSCD (a) and the Fourier pseudospectral method (b).

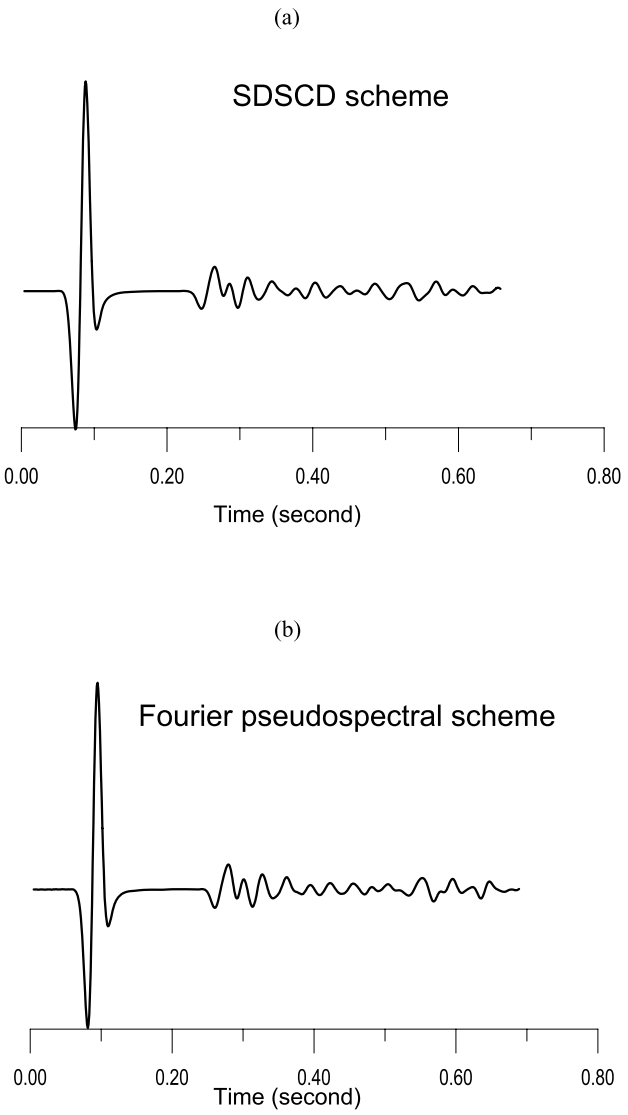

Figure 7. Comparison of synthetic seismograms (vertical component) for a lateral heterogeneous medium model generated by the SDSCD (a) and the Fourier pseudospectral method (b).

We now consider a more complex case consisting of the Marmousi model (Fig. 8). It is such a representative model (Versteeg 1993) that can be used to describe strongly heterogeneous media including continuous and discontinuous parameter changes. In the model, it is supposed that the *S*-wave velocity structure ranges from 1500 to 5500 m s^{-1} and the *P*-wave velocity of $V_P = \sqrt{3}V_S$. The number of gridpoints is 384 × 122, the model size was 7680 m × 2440 m, and the pressure source was located at $(x_s, z_s) = (3840$ m, -200 m), which is a Ricker wavelet (eq. 18) with an amplitude spectrum peak at 25 Hz. The spatial increment is 20 m and the time increment was 2 ms.

Figs 9(a) and (b) are snapshots of elastic wavefields for the vertical component at time marks of 400 ms generated by the SDSCD and by the Fourier pseudospectral scheme, respectively. Comparing the numerical results, it can be found that there is hardly any evidence of numerical dispersion in the SDSCD approach just as in the Fourier pseudospectral scheme. The above-mentioned comparison indicates that the SDSCD is likewise efficient in strongly heterogeneous media.

To test the long-time performance of the SDSCD scheme, we compared the numerical results computed by SDSCD with those from Fourier pseudospectral scheme for a 2-D homogeneous medium model. The model parameter were a *P*-wave velocity of $V_P = 3000$ m s^{-1}, a *S*-wave velocity of $V_S = 1732$ m s^{-1} and a density of $\rho = 2400$ kg m^{-3}. The number of gridpoints was 256 × 256, the model size was 5100 m × 5100 m, and the pressure source was located at $(x_s, z_s) = (2550$ m, 2550 m), which was a Ricker wavelet (see eq. 18) with an amplitude spectrum peak at 30 Hz. The spatial increments were 20 m and the time increment was 2 ms. This was a medium model without any type of absorbing or transmitted boundary conditions.

Figs 10(a)–(c) show elastic wavefield (vertical component) snapshots generated by the SDSCD scheme after 400, 2000 and 5000 time steps, respectively. Similarly, Figs 10(d)–(f) display elastic wavefield snapshots generated by the Fourier pseudospectral scheme after 400, 2000 and 5000 time steps, respectively. From Figs 10(a) and (d), it can be found that the wave front curves generated by the two schemes after 400 time steps are quite clear. For short-time numerical simulations, therefore, they have similar performance in the same case. For long-time numerical simulations, however, the aforementioned two schemes perform quite differently and have different error growth. After 2000 times steps (4000 ms), it can be observed that the SDSCD scheme has slightly numerical dispersion, whereas the Fourier pseudospectral scheme suffers obvious numerical dispersion. The CPU (Core 2 Duo 2.53 GHz) time for the SDSCD scheme and the Fourier pseudospectral scheme is 672.25 and 299.83 s, respectively. Although the CPU time required by the Fourier pseudospectral scheme is less than that required by the SDSCD scheme, the Fourier pseudospectral scheme suffers obvious numerical dispersion. On a fine grid ($\Delta x = \Delta z = 10$ m, $\Delta t = 1$ ms), the CPU time required by the Fourier pseudospectral scheme soars

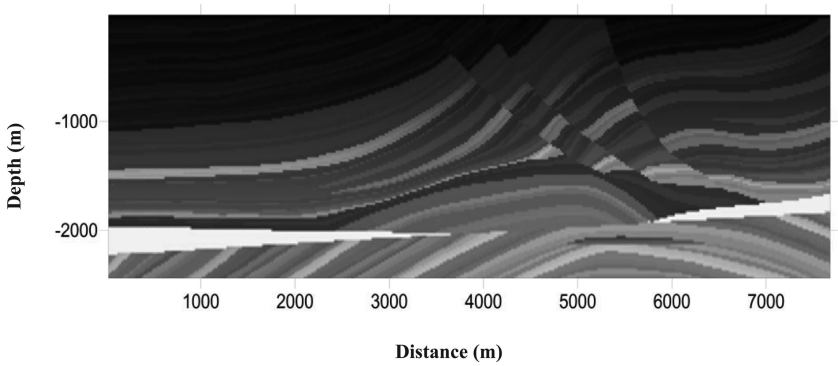

Figure 8. Marmousi model: configuration.

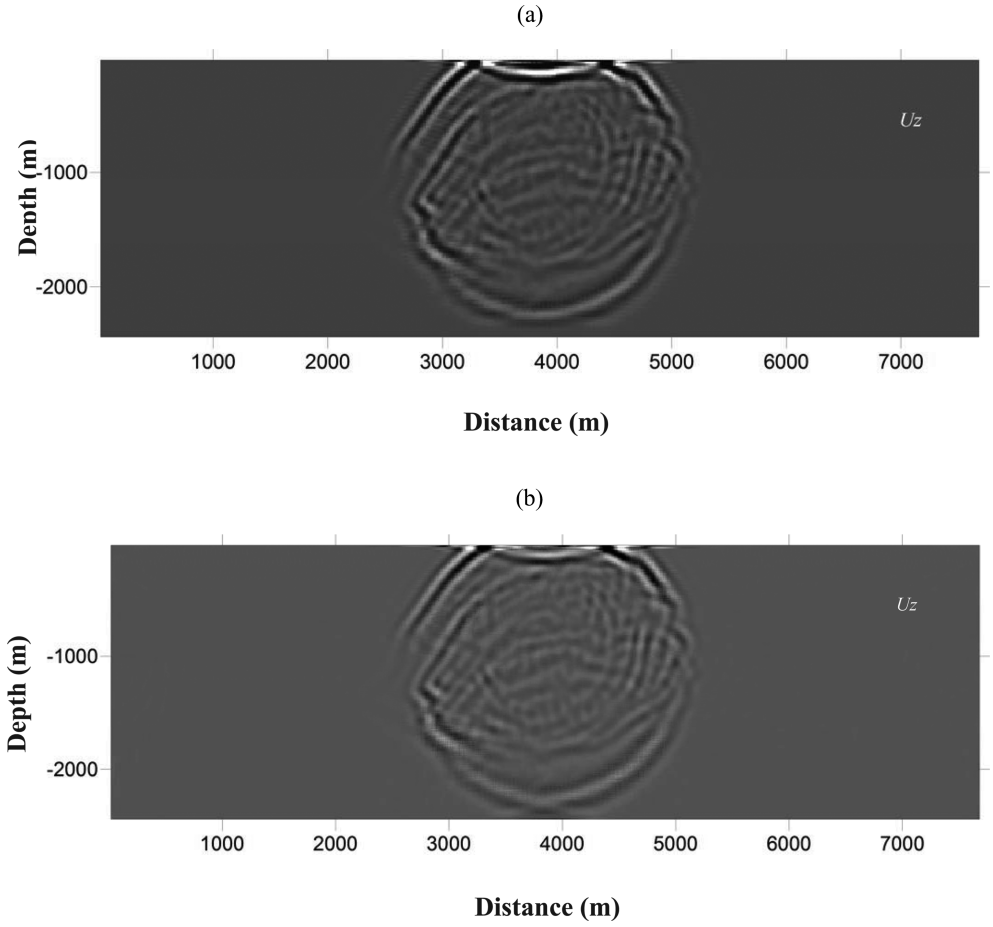

Figure 9. Snapshots of elastic wavefield for the vertical component in the Marmousi model at time marks of 400 ms generated by the SDSCD (a) and the Fourier pseudospectral scheme (b).

to 3435.03 s and numerical dispersion reduces markedly (Fig. 10g). Under the same condition of eliminating the numerical dispersion, computational CPU time of the SDSCD scheme is about 19.57 per cent of that of the Fourier pseudospectral scheme and computer memory required by the SDSCD scheme is about 25 per cent of that required by the Fourier pseudospectral scheme. After 5000 time steps, the wave front curves computed by the SDSCD scheme are still clearly seen. At this time, however, the wave front curves computed by the Fourier pseudospectral scheme have blurred seriously. This comparison indicates that the two schemes perform very differently for long-time computation, and the SDSCD scheme is very suitable for long-time simulation. The comparison also indicates that the computational efficiency of the SDSCD scheme is superior to that of the Fourier pseudospectral scheme for long-time simulation and the SDSCD can greatly save both computational CPU time and computer memory via using the coarse spatial and large time steps.

CONCLUSIONS

In this paper, an alternative method for structure-preserving modelling of elastic waves has been presented, which is based on a third-order SDSCD scheme. For temporal discretizations, the SDSCD method is a structure-preserving scheme. Theoretically, it can be applied to long-time simulations. For spatial discretizations, nine-point operators on regular grids are designed for optimizing the computational efficiency and accuracy of the presented approach. The nine-point SDSCD is a localized operator that can describe the local properties of complicated wavefields and avoid non-causal interaction of the propagating wavefield when parameter discontinuities are present in the medium. This approach is therefore suitable for large-scale numerical modelling since it effectively suppresses numerical dispersion by discretizing the wave equations when coarse grids are used. Because the SDSCD approach is equivalent to an optimized FD method in nature, it is suitable to any type of absorbing or transmitted boundary condition that is suitable for conventional FD methods. Although the approach presented is only applied to the 2-D elastic wavefield calculation for heterogeneous models and to long time simulation of the 2-D elastic wavefield in this paper, it can be readily extended to 3-D elastic wavefield calculations.

From the simulation results in this paper, it has been shown that the SDSCD method can effectively capture the inner interface without any special treatment at the discontinuity; therefore, it can simulate seismic waves in complicated geometries and highly heterogeneous media without any additional treatment. The SDSCD allows us to use a coarse grid, that is, fewer samples per wavelength, to achieve the same accuracy in modelling waves and is similar to that obtained by conventional FD schemes on a finely sampled grid. As a result, the SDSCD can greatly save both computational CPU time and computer memory via using the coarse spatial and large time steps. The numerical experiments also demonstrate the remarkable ability of the SDSCD for long-time simulation of elastic

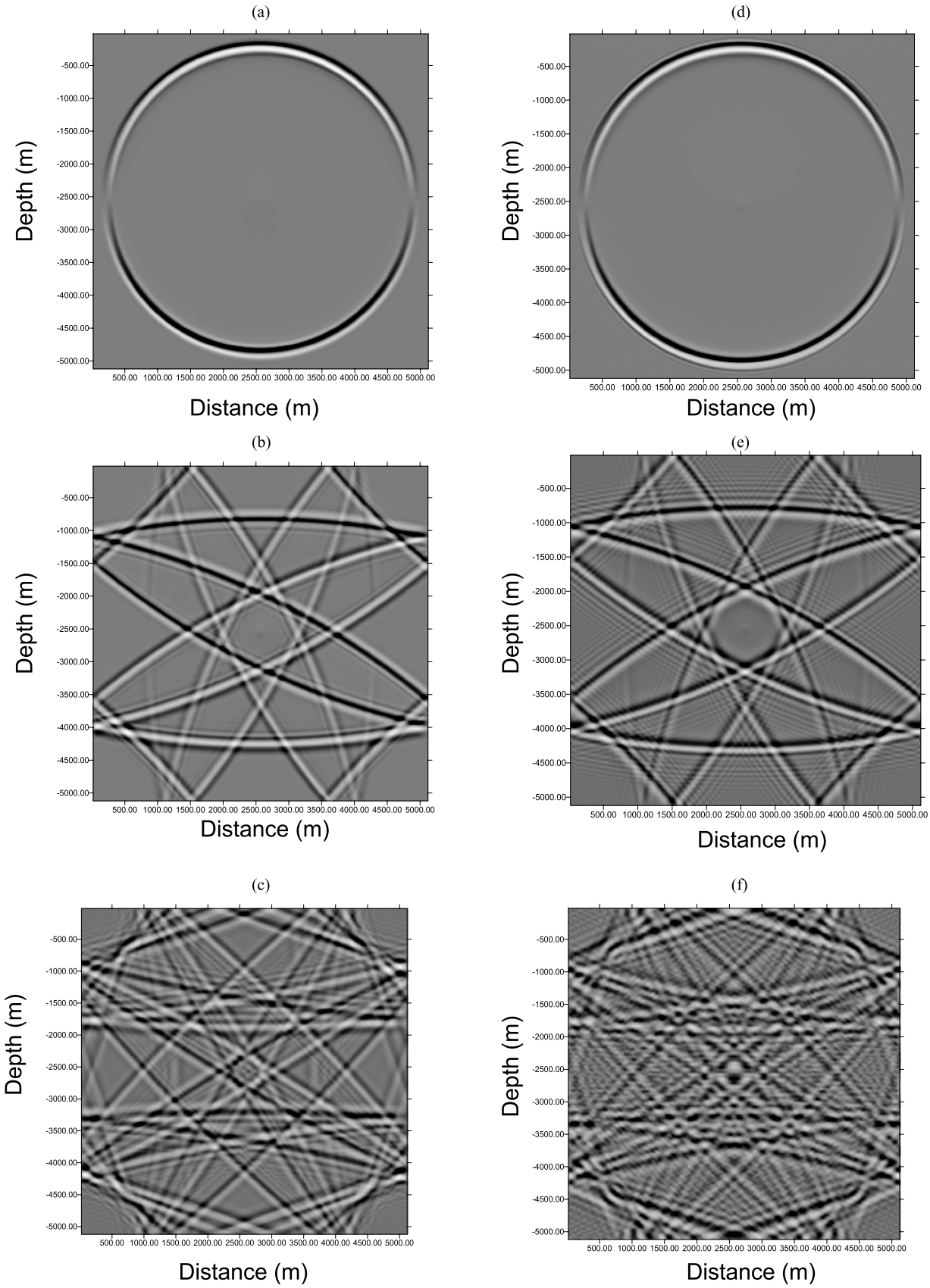

Figure 10. Snapshots of elastic wavefields (vertical component) in a 2-D homogeneous medium model generated by SDSCD after (a) 400 time steps, (b) 2000 time steps (4 s) and (c) 5000 time steps. Snapshots of elastic wavefields in the same medium model generated by the Fourier pseudospectral method after (d) 400 time steps, (e) 2000 time steps, (f) 5000 time steps and (g) 4 s (for $\Delta x = \Delta z = 10$ m, $\Delta t = 1$ ms).

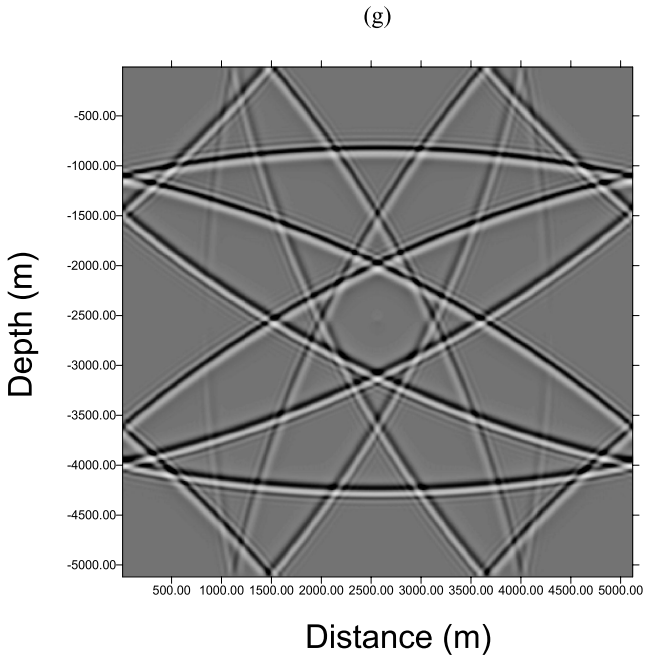

Figure 10. (*Continued.*)

equations. The results here hold promise not only for future seismic wave studies, but also for any geophysical research that requires structure-preserving numerical solution (or long-time simulations) of partial differential equation with variable coefficients. Although the concept of the SDSCD seems not to be very new mathematically, a structure-preserving solution of elastic wave equations is obtained by using the SDSCD presented by this paper and it is very suitable for high-precision modelling of elastic wavefield, especially for its long-time simulations. This is exactly what new meaning of this paper is about. So far no reference on similar research has been found.

ACKNOWLEDGMENTS

This work has been supported by the National Natural Science Foundation of China (Grant No. 40437018, 40874024, 41174047) and The Ministry of Science and Technology of People's Republic of China (973 Project, Grant No. 2007CB209603).

REFERENCES

Bayliss, A., Jordan, K.E., LeMesurier, B.J. & Turkel, E., 1986. A fourth-order accurate finite-difference scheme for the computation of elastic waves, *Bull. seism. Soc. Am.,* **76,** 1115–1132.

Blanes, S. & Moan, P.C., 2002. Practical symplectic partitioned Runge-Kutta and Runge-Kutta-Nyström methods, *J. comput. appl. Math.,* **142,** 313–330.

Calvo, M.P. & Sanz-Serna, J.M., 1993. High-order symplectic Runge-Kutta-Nyström methods, *SIAM J. Scient. Comput.,* **14,** 1237–1252.

Carcione, J.M., Herman, G.C. & Kroode, A.P.E. ten, 2002. Seismic modeling, *Geophysics,* **67,** 1304–1325.

Cerjan, C., Kosloff, D., Kosloff, R. & Reshef, M., 1985. A nonreflecting boundary condition for discrete acoustic and elastic wave equations, *Geophysics,* **50,** 705–708.

Chen, H.W., 1996. Staggered grid pseudospectral simulation in viscoacoustic wavefield simulation, *J. acoust. Soc. Am.,* **100,** 120–131.

Chen, J.B., 2009. Lax-Wendroff and Nyström methods for seismic modeling, *Geophys. Prospect.,* **57,** 931–941.

Chen, J.B. & Qin, M. Z., 2000. Ray Tracing by symplectic algorithm, *Numer. Comput. Comput. Appl.* (in Chinese), **4,** 255–265.

Ciarlet, P.G. & Lions, J.L., 1991. *Handbook of Numerical Analysis,* North-Holland, Amsterdam.

Claerbout, J.F., 1985. *Imaging the Earth's Interior,* Blackwell Science, Inc, Oxford.

De Hoop, A., 1960. A modification of Cagniard's method for solving seismic pulse problems, *Appl. Sci. Res. B.,* **8,** 349–356.

Dormy, E. & Tarantola, A., 1995. Numerical simulation of elastic wave propagation using a finite volume method, *J. geophys. Res.,* **100,** 2123–2133.

Etgen, J.T., 1987. Finite-difference elastic anisotropic wave propagation, *Stanford Explor. Project,* **56,** 23–57.

Feng, B.F. & Wei, G.W., 2002. A comparison of the spectral and the discrete singular convolution schemes for the KdV-type equations, *J. Comput. Appl. Math.,* **145,** 183–188.

Fornberg, B., 1990. High order finite differences and pseudospectral method on staggered grids, *SIAM J. Numer. Anal.,* **27,** 904–918.

Gazdag, J., 1981. Modeling of the acoustic wave equation with transform methods, *Geophysics,* **46,** 854–859.

Geller, R.J. & Takeuchi, N., 1998. Optimally accurate second-order time-domain finite difference scheme for the elastic equation of motion: one-dimensional case, *Geophys. J. Int.,* **135,** 48–62.

Gottlieb, D., Lustman, L. & Orszag, S.A., 1981. Spectral calculations of one dimensional, inviscid compressible flow, *SIAM J. Sci. Statist. Comput.,* **2,** 296–310.

Hairer, E., Nøsett, S.P. & Warnner, G., 1993. *Solving Ordinary Differential Equations I,* Springer-Verlag, Berlin.

Holberg, O., 1987. Computational aspects of the choice of operator and sampling interval for numerical differentiation in large-scale simulation of wave phenomena, *Geophys. Prospect.,* **35,** 629–655.

Iwatsu, R., 2009. Two new solutions to the third-order symplectic integration method, *Phys. Lett. A,* **373,** 3056–3060.

Komatitsch, D. & Tromp, J., 2002. Spectral-element simulation of global seismic wave propagation—I. Validation, *Geophys. J. Int.,* **149,** 390–412.

Komatitsch, D. & Vilotte, J.P., 1998. The spectral element method: an efficient tool to simulate the seismic response of 2D and 3D geological structures, *Bull. seism. Soc. Am.,* **88,** 368–392.

Lax, P.D. & Wendroff, B., 1960. System of conservation laws. *Commun. Pure appl. Math.,* **13,** 217–237.

Lunk, C. & Simen, B., 2005. Runge-Kutta-Nyström methods with maximized stability domain in structural dynamics. *Appl. Numer. Math.,* **53,** 373–389.

Levander, A.R., 1988. Fourth-order finite-difference *P-SV* seismograms, *Geophysics,* **53,** 1425–1435.

Moczo, P., Kristek, J., Vavrycuk, V., Archuleta, R.J. & Halada, L., 2002. 3D heterogeneous staggered-Grid finite-difference modeling of seismic motion with volume harmonic and arithmetic averaging of elastic moduli and densities, *Bull. seism. Soc. Am.,* **92,** 3042–3066.

Mora, P., 1986. Elastic finite-difference with convolutional operators, *Stanford Explor. Project,* **48,** 272–289.

Okunbor, P.J. & Skeel, R.D., 1992. Canonical Runge-Kutta-Nyström methods of orders 5 and 6, Working paper 92–1, Department of Computer Science, University of Illinois.

Qian, L., 2003. On the regularized Whittaker-Kotel'nikov-Shannon sampling formula, *Pro. Am. Math. Soc.,* **131**(4), 1169–1176.

Qin, M.Z. & Zhu, W.J., 1991. Canonical Runge-Kutta-Nyström methods for second order ODE's, *Comput. Math. Appl.,* **22,** 85–95.

Sun, Y.H. & Zhou, Y.C., 2006. A windowed Fourier pseudospectral method for hyperbolic conservation laws. *J. comput. Appl. Math.,* **214**(2), 466–490.

Suzuki, M., 1992. General theory of higher-order decomposition of exponential operators and symplectic integrators, *Phys. Lett. A,* **165,** 387–395.

Takeuchi, N. & Geller, R.J., 2000. Optimally accurate second-order time-domain finite difference scheme for computing synthetic seismograms in 2-D and 3-D media, *Phys. Earth planet. Inter.,* **119,** 99–131.

Tsitouras, Ch., 1999. A tenth-order symplectic Runge-Kutta-Nyström method, *Celest. Mech. Dyn. Astron.,* **74,** 223–230.

Versteeg, R.J., 1993, Sensitivity of prestack depth migration to the velocity model, *Geophysics,* **58,** 873–882.

Virieux, J., 1986. P-SV wave propagation in heterogeneous media: velocity-stress finite-difference method, *Geophysics,* **51,** 889–901.

Yang, S.Y., Zhou, Y.C. & Wei, G.W., 2002. Comparison of the discrete singular convolution algorithm and the Fourier pseudospectral method for solving partial differential equations, *Comput. Phys. Comm.,* **143,** 113–135.

Yang, D.H., Lu, M., Wu, R.S. & Peng, J.M., 2004. An optimal nearly analytic discrete method for 2D acoustic and elastic wave equations, *Bull. seism. Soc. Am.,* **94,** 1982–1991.

Yoshida, H., 1990. Construction of higher order sympletic integrators, *Phys. Lett. A,* **150,** 262–269.

Yomogida, K. & Etgen, J.T., 1993. 3-D wave propagation in the Los Angeles Basin for the Whittier-Narrows earthquake, *Bull. seism. Soc. Am.,* **83,** 1325–1344.

Zhao, Z., Xu, J. & Shigeki, H., 2003. Staggered grid real value FFT differentiation operator and its application on wave propagation simulation in the heterogeneous medium. *Chin. J. Geophys.,* **46**(2), 234–240 (in Chinese).

Zhou, B. & Greenhalgh, S.A., 1992. Seismic scalar wave equation modeling by a convolutional differentiator, *Bull. seism. Soc. Am.,* **82,** 289–303.